*Desalination and Water Treatment*
www.deswater.com

doi: 10.5004/dwt.2017.21104

85 (2017) 120–131
August

# Study of the hydrogeochemical processes during enhanced trimethoprim and sulfamethoxazole removal in artificial composite soil treatment system

Qinqin Liu[a,b], Miao Li[a,*], Fawang Zhang[c], Hechun Yu[d], Quan Zhang[a], Xiang Liu[a,*]

[a]*School of Environment, Tsinghua University, Beijing 100084, China, Tel. +86 010 6279 7667; emails: miaoli@tsinghua.edu.cn (M. Li), x.liu@tsinghua.edu.cn (X. Liu), liuqq2008@163.com (Q. Liu)*
[b]*The Institute of Crustal Dynamics, China Earthquake Administration, Beijing 100085, China, Tel. +86 18813181173; email: 1308342539@qq.com (Q. Liu)*
[c]*Chinese Academy of Geological Sciences, Beijing 100037, China, Tel. +86 187 0773 7886, email: zhangfawang@karst.ac.cn*
[d]*China University of Geosciences (Beijing), Beijing 100083, China, Tel. +86 150 0125 8016, email: 923026136@qq.com*

Received 31 March 2017; Accepted 27 June 2017

**ABSTRACT**

The removal of trimethoprim (TMP) and sulfamethoxazole (SMX) by column experiments was systematically investigated, in which an artificial composite soil treatment system (ACST) simulating irrigation soils at high infiltration rates (>89.11 m $d^{-1}$) was constructed. The levels of $K^+$, $Na^+$, $Ca^{2+}$, $Mg^{2+}$, $Fe^{3+}$, $Mn^{2+}$, $Cu^{2+}$, and $Zn^{2+}$ during hydrogeochemical processes were focused in this study. The results demonstrate that ACST with high infiltration rates improved the removal of SMX and TMP, with removal rates about 20% higher than the removal rates of transitional sands. Moreover, under the condition of the same ACST infiltration rate, the removal rate of TMP was higher than that of SMX. This shows that influent high $Na^+$ concentrations might directly hinder the release of $Ca^{2+}$, while $Ca^{2+}$ might participate in SMX and TMP removal. The results also show that a small portion of the $K^+$ released from dissolution were derived from soil desorption and participated in the removal of TMP and SMX. On the whole, SMX and TMP removal processes are related with hydrogeochemical processes of $K^+$, $Na^+$, $Ca^{2+}$, and $Mg^{2+}$. Effluent $Fe^{3+}$, $Mn^{2+}$, $Cu^{2+}$, and $Zn^{2+}$ concentrations were on the μg $L^{-1}$ level. In this study, the ACST is determined to be a suitable method for the treatment of water contaminated with SMX and TMP.

*Keywords:* Trimethoprim; Sulfamethoxazole; Hydrogeochemical processes; Ion exchange

## 1. Introduction

Managed aquifer recharge systems such as river bank filtration (RBF) are used globally to treat surface water. RBF is a process during which river water is subjected to subsurface flow [1]. River water is naturally filtered by passing through the riverbed and aquifer. The bank filtrate is diluted by groundwater. The target of RBF is to remove constituents such as bacteria, protozoa, pathogens, natural organic matter, and turbidity. However, the effectiveness of removing antibiotics by RBF is unclear. In particular, the removal of sulfonamides, which are not easily adsorbed or degraded, has not been well examined. The presence and fate of antibiotics during RBF merits further attention.

Sulfamethoxazole (SMX) and trimethoprim (TMP) are also two critical pharmaceuticals in RBF due to its enhanced persistency compared with other antibiotics. Municipal wastewater treatment plants fail to eliminate sulfonamide antibiotics (SMX/TMP) [2], and discharge of effluent containing these compounds is a major source of river water pollution. It is proved that SMX and TMP have the ability to reach receiving surface water systems, since they are not completely removed during conventional wastewater treatment [3,4]. In this study, the removal of SMX and TMP was investigated together. It is difficult to provide appropriate post-treatment after RBF to create an adequate or even absolute barrier against SMX and TMP in drinking water

* Corresponding author.

1944-3994/1944-3986 © 2017 Desalination Publications. All rights reserved.

treatment plants. Thus, it is significant to use our artificial composite soil treatment system (ACST) simulating RBF as a barrier against SMX and TMP to improve the SMX and TMP removal rates. In this study, ACST simulating RBF was set up in the laboratory to remove SMX and TMP.

Most water treatment technologies used for the removal of pharmaceuticals, especially antibiotics, aim for high removal rates and do not account for hydrogeochemical processes, which are key to ensuring basic water quality. The complexation of cations, where ions chemically bond with water molecules, leads to the creation of complex ions of fixed composition and high chemical stability [5]; this is particularly true for the transition metals such as iron, copper, and zinc. However, most antibiotics such as quinolones, sulfonamides, and tetracyclines are ionic compounds; this might be related to hydrogeochemical processes of inorganic compounds. Additionally, chemical and biochemical interactions between water, soils, and rocks produce a variety of dissolved inorganic and organic constituents. There are also various processes, such as the weathering of carbonate and silicate, the dissolution of sulphate minerals, pyrite oxidation, and evaporative dissolution, responsible for the production of dissolved ions [6,7]. However, no documented work is available on hydrogeochemical processes in soil treatment systems. Thus, for drinking water companies that operate RBF systems, such as those in Berlin (Germany) and the Netherlands, where drinking water production relies primarily on bank filtration, it is important to improve the removal rate of antibiotics by simulating RBF. Simultaneously, hydrogeochemical processes should also be payed enough attention.

Clay ceramsites are highly efficient, inexpensive, and easily acquired; they also have a demonstrated sorption capability for sulfonamides. For this study, we chose clay ceramsites as the primary material for sulfonamide removal, and used silty clay and medium-coarse sands to simulate RBF. ACST about RBF was built to remove sulfonamides (SMX and TMP). To the best of our knowledge, hydrogeochemical indexes, such as $K^+$, $Na^+$, $Ca^{2+}$, $Mg^{2+}$, $Fe^{3+}$, $Mn^{2+}$, $Cu^{2+}$, and $Zn^{2+}$, have not been reported previously in such systems. However, for ionizable compounds such as SMX and TMP, these hydrogeochemical indexes might not only affect the final water quality but also help to explain the mechanism about the removal of SMX and TMP in soil.

## 2. Experimental section

### 2.1. Chemicals and reagents

The chemicals used, suppliers, and purities are described in the supplementary. Physicochemical properties of the sulfonamide antimicrobials are listed in Table 1. Sulfonamide antimicrobials possess two ionizable functional groups relevant to the environmental pH range: the anilinic amine and the amide moieties [8]. The cationic species dominates at low pH values; the neutral form is the principal species at pH values between pKa1 and pKa2.

### 2.2. Preparation of ACST studies

An overview of the ACST set-up is given in Fig. 1. Three polymethyl methacrylate ACSTs (height, 65 cm; outside diameter, 10 cm; inside diameter, 9 cm; base plate, 121 $cm^2$) with no SMX/TMP loss were set up to conduct the removal of SMX and TMP in the laboratory. Results of the elemental analysis of the three kinds of material are described in Table 2. The detailed sampling process, the packing process of columns, and the pretreatment process of columns are described in the supplementary and Table 3. The SMX and TMP limits of detection are 0.4 and 0.3 μg $L^{-1}$, respectively. However, the SMX and TMP environment concentrations are at low (μg $L^{-1}$) levels. For ensuring the effluent concentration to be detected during the experimental process and representing the actual environmental concentration, 20–30 μg $L^{-1}$ influent SMX and TMP concentrations were chosen. The prepared 20–30 μg $L^{-1}$ SMX and TMP solutions were pumped at a flow rate of 5 mL $min^{-1}$ and with

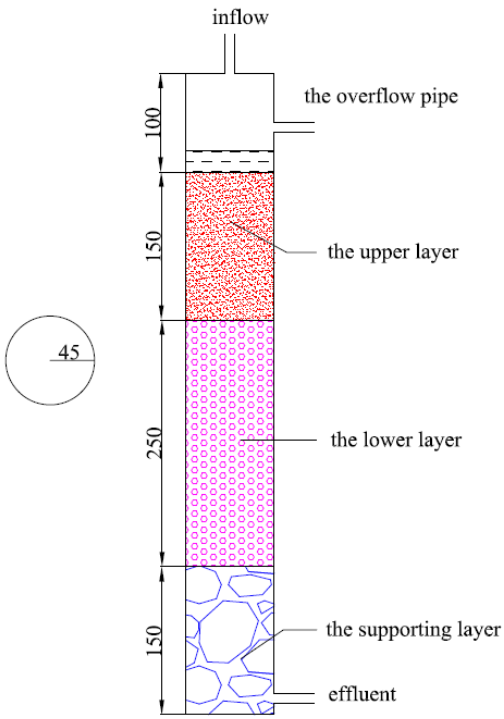


Fig. 1. Schematic diagram of the artificial composite soil column. The values are given in millimeter.

Table 1
Physicochemical properties of SMX and TMP

| Chemicals | Molecular formula | CAS# | Molecular weight | Water solubility (mg $L^{-1}$ at 25°C) | Log Kow | pKa1/pKa2 |
|---|---|---|---|---|---|---|
| SMX | $C_{10}H_{11}N_3O_3S$ | 723-46-6 | 253.28 | 410 | 0.90 | 1.60/5.70 [8] |
| TMP | $C_{14}H_{18}N_4O_3$ | 738-70-5 | 290.32 | <1,000 | 0.91 | 3.24/6.76 [8] |

Table 2
Elemental analysis results of clay ceramsites, silty clay, and medium-coarse sands

| | $SiO_2$ (%) | $Al_2O_3$ (%) | MgO (%) | CaO (%) | $Na_2O$ (%) | $K_2O$ (%) | $Fe_2O_3$ (%) | MnO (%) | ZnO (%) | CuO (%) | Others (%) |
|---|---|---|---|---|---|---|---|---|---|---|---|
| Clay ceramsites | 56.28 | 15.78 | 0.76 | 9.29 | 0.09 | 2.25 | 15.38 | 0.13 | 0.03 | 0.01 | 0.10 |
| Silty clay | 71.48 | 9.72 | 1.43 | 6.71 | 1.00 | 2.86 | 5.50 | 0.09 | 0.01 | 0 | 1.20 |
| Medium-coarse sands | 79.32 | 9.52 | 0.36 | 1.87 | 1.42 | 4.66 | 2.19 | 0.05 | 0 | 0 | 0.61 |

Table 3
ACST packing experimental scheme

| ACST codes | ACST 1 | ACST 2 | ACST 3 |
|---|---|---|---|
| Upper layer | Medium-coarse sands : silty clay (v:v) = 10:1 | Medium-coarse | Medium-coarse sands : silty clay (v:v) = 10:1 |
| Lower layer | Clay ceramsites | Clay ceramsites | Clay ceramsites |
| Supporting layer | Cobblestones | Cobblestones | Cobblestones |

hydraulic loading of 1.13 m $d^{-1}$ in columns 1–3. The influent of column 3 was added 200 mg $L^{-1}$ $NaN_3$ to inhibit the growth of microorganisms during the experimental process. The laboratory temperature is about 20°C. Each sample was tested twice and the average values of detected results were used in this study. The batch experiments about the SMX and TMP sorption on clay ceramsites are described in the supplementary.

### 2.3. Analytical methods

Samples were analyzed by liquid chromatography with tandem mass spectrometry (UPLC/MS/MS) using a LCQ advantage ion trap mass spectrometer equipped with an electrospray ionization source operated in positive ion mode (Waters, USA). A Waters ACQUITY BEH $C_{18}$ column, 1.7 μm, 2.1 × 50 mm ACST was used. The flow rate was 0.25 mL $min^{-1}$. The gradient elution program and the antibiotics working parameters in mass spectrum are shown in Tables S1 and S2 in the supplementary. Oven temperature of the ACST was 30°C, and the full loop injection volume was 2 μL. Quantification of TMP and SMX was performed in MRM mode (Multiple Reaction Monitoring). 500 L $h^{-1}$ gas flow, 120°C source temperature, and 2.6 kV capillary are the working conditions of mass spectrum. The working parameters of antibiotics in mass spectrum were listed in the supplementary. pH and dissolved oxygen (DO) were tested using potable water quality analyzer (HACH, USA). Cations ($K^+$, $Ca^{2+}$, $Na^+$, and $Mg^{2+}$) were tested using ion chromatography method [9]. Trace elements ($Fe^{3+}$, $Mn^{2+}$, $Cu^{2+}$, and $Zn^{2+}$) were tested using ICP/MS method [10]. Potentiometric titration method, EDTA titration method, and Brunauer–Emmett–Teller (BET) method were used to test zero point charge, cation exchange capacity (CEC), and specific surface area of clay ceramsites, respectively. The testing results were listed in Table 4.

## 3. Results and discussion

### 3.1. Variability of organic sulfonamide removal over time

The concentrations of SMX and TMP were monitored in these ACSTs with different infiltration rates in Table 5, fed with 20–30 μg $L^{-1}$ SMX and TMP deionized solutions. The influent and effluent concentrations of SMX and TMP are described in Figs. 2(a) and (b), respectively. The removal rates of SMX and TMP are described in Figs. 2(c) and (d), respectively.

Table 4
Physicochemical property of clay ceramsites

| Sample | pH | $pH_{zpc}$ | O (%) | CEC (cmol $kg^{-1}$) | BET ($m^2$ $g^{-1}$) |
|---|---|---|---|---|---|
| Clay ceramsites | 9.70 | 4.32 | 0.49 | 7.00 | 18.80 |

Note: "O" represents organic matter content.

The SMX removal results showed that the removal rates for columns 1 and 3 were comparable while the removal rate of column 2 was low. The sorption capacity of silty clay is slightly better than medium-coarse sands, thus the removal efficiency of columns 1 and 3 was better than column 2. It was reported that no significant removal was observable in columns filled with sands [11]. However, in this study, the average removal rate for column 2 filled with medium-coarse was 28.7%, which is reasonable to confirm the important role of clay ceramsites in the SMX removal process. By batch experiments, the SMX sorption capacity of clay ceramsites was 51.85 μg $g^{-1}$. Compared with the column experiments, the removal rate of column 2 was obviously lower. It could be related to the infiltration rate. In this study, high infiltration rate is the character of ACST, so it is possible that the high infiltration rate (217.99 m $d^{-1}$) of column 2 affected the removal efficiency. Many studies also suggested that long hydraulic retention time results in higher removal efficiency [4,11,12]. For columns 1 and 3, two factors may account for an increase in SMX removal: (a) the added silty clay in columns 1 and 3 and (b) the lower infiltration rate than column 2. Though column 1 (94.63 m $d^{-1}$) and column 3 (89.11 m $d^{-1}$) had a relatively low infiltration rate, it is also obviously higher than other experiments [13,14]. In such short hydraulic retention time, the average removal rate for columns 1 and 3 still achieves 49.36% and 45.68%. Columns 1 and 3 were filled

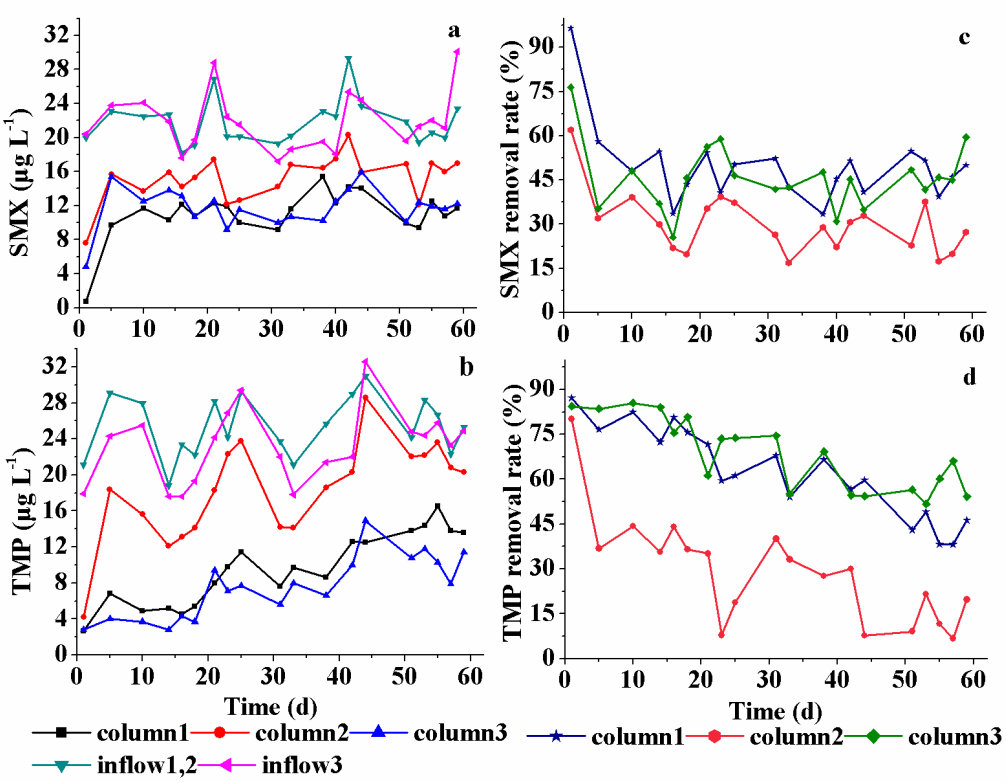


Fig. 2. The influent concentrations, effluent concentrations, and the removal rates of SMX and TMP. (a) and (b) represent the influent and effluent concentrations of SMX and TMP, respectively. Columns 1–3 represent the SMX and TMP effluent concentrations of columns 1–3, respectively. Inflow 1,2 represents the SMX and TMP influent concentrations of columns 1 and 2. Inflow 3 represents the SMX and TMP influent concentrations of column 3. (c) and (d) represent the removal rates of SMX and TMP, respectively. Columns 1–3 represent the SMX and TMP removal rates of columns 1–3, respectively.

with the same material, but column 3 was fed with 200 mg $L^{-1}$ $NaN_3$ to inhibit the growth of microorganisms. From removal results, the average SMX removal rate of column 3 was a little higher than column 1 (it is possible that personal errors occurred in the packing of columns), so biodegradation in column 1 was very weak. This phenomenon also reflected that sulfonamides were difficult to be degraded [15], which agreed with the results of the long-time adaptation of SMX [11]. From pH monitoring results, it can be seen that initial pH fluctuated between 6 and 7, as depicted in Fig. 3(a). The pKa values of SMX were 1.6 and 5.7 respectively. SMX is a kind of amphoteric compound and exists with the form of molecules or ions in different pH conditions. Therefore, under influent of pH conditions, SMX mainly exists in the form of molecules and anions in water. After the influent was through columns, some SMX were removed. It is possible that the hydrophobic effect is the main sorption mechanism in the removal process of SMX molecular forms because clay ceramsites contain some organic matter. Using scanning electron microscope technique to observe the surface of clay ceramsites, depicted in Fig. 4, developed internal pore structures of clay ceramsites were observed. The specific surface area of clay ceramsites is 18.80 $m^2$ $g^{-1}$. Therefore, it is possible that the pore filling is also the main sorption mechanism. While influent was changed to deionized water without SMX, effluent pH values of three columns were not obviously different. It is possible that the effluent pH variation is not related to the removal of SMX.

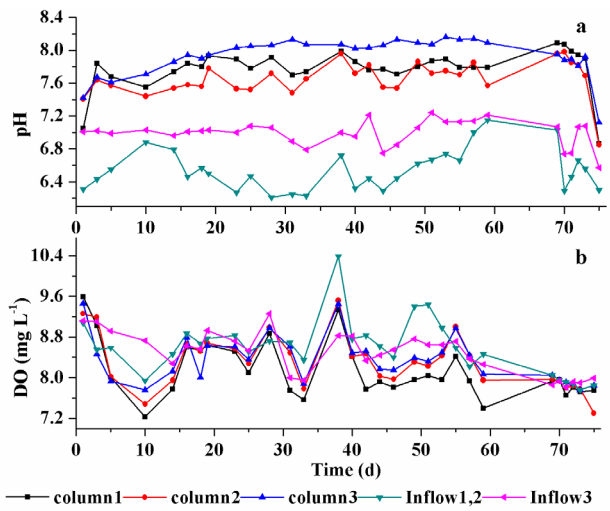


Fig. 3. The variability of pH and DO over time. (a) represents the pH variability over time. Inflow 1,2 represents the influent pH variabilities of columns 1 and 2. Inflow 3 represents the influent pH variability of column 3. Columns 1–3 represent the effluent pH variabilities of columns 1–3, respectively. (b) represents the DO variability over time. Inflow 1,2 represents the influent DO variabilities of columns 1 and 2. Inflow 3 represents the influent DO variability of column 3. Columns 1–3 represent the effluent DO variabilities of columns 1–3, respectively.

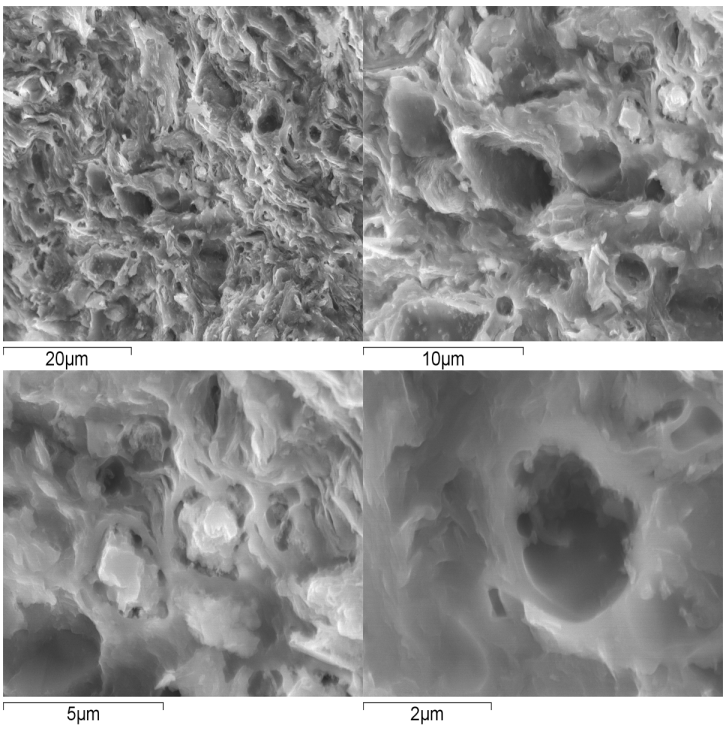


Fig. 4. The scanning electron micrograph of clay ceramsites.

TMP removal was investigated in lab-scale columns over a period of 60 d. The TMP removal rate agreed with that of SMX, and the removal rates of columns 1 and 3 were comparable, though the removal of TMP was slightly better than SMX. Columns 1 and 3 were filled with the same material, but the influent of column 3 was also supplemented with $NaN_3$ (200 mg $L^{-1}$) to inhibit the growth of microorganisms. The average removal rate of column 3 (68.35%) was slightly higher than that of column 1 (62.46%), indicating that microbial degradation was weak and that sorption might be the main removal mechanism. From the result of pH monitoring, it can be seen that the initial pH fluctuated between 6 and 7, as depicted in Fig. 3(a). The pKa values of TMP were 3.24 and 6.76, respectively. Under influent pH conditions, TMP mainly exists in the form of molecules and anions in water. The hydrophobic effect, developed internal pore structure and high specific surface area of clay ceramsites might help adsorb TMP. TMP effluent concentrations increased slightly over time in three columns, that is, the removal rates decreased slowly over that period. The SMX and TMP removal amount from three columns during 60-d experiment was listed in the Table 6. It is obvious that the removal amount of SMX and TMP in column 2 is comparative and less than those of columns 1 and 3. According to the result of batch experiments, the sorption capacities of TMP and SMX are 151.82 and 51.85 μg $g^{-1}$, respectively. However, the amount of clay ceramsites added in every column was about 1,533.32 g. Thus, the sorption capacities of SMX and TMP in every column are about 79.44 and 232.59 g, respectively. Obviously, the total removal amount of SMX and TMP is less than the amount of SMX and TMP sorption capacity. There might be two factors. One factor is the sorption time. The sorption time is longer in batch experiments than in column experiments, because all the samples were orbitally shaken at 150 rpm in batch experiments.

Table 5
Average infiltration rates and porosities of three columns

| | Column 1 | Column 2 | Column 3 |
|---|---|---|---|
| Infiltration rate (m $d^{-1}$) | 94.63 | 217.99 | 89.11 |
| Average porosity | 0.28 | 0.29 | 0.28 |

Table 6
Total removal amount of columns 1–3 during 60-d experiments

| Removal amount (g) | Column 1 | Column 2 | Column 3 |
|---|---|---|---|
| SMX | 46.57 | 28.38 | 43.74 |
| TMP | 64.76 | 29.16 | 64.56 |

The other factor is contact area. In the batch experiments, there is a good contact area between clay ceramsites and the solution with SMX and TMP by shaking ground-glass conical flask at 150 rpm. However, in the column experiments, the droplets falling to the columns with gravity result in the limited contact area. DO is an important parameter in assessing water quality, referring to the level of free, non-compound oxygen present in water. From DO monitoring, as depicted in Fig. 3(b), influent DO concentrations of three columns were slightly higher than the effluent'. It is related to the high influent flow rate (5 mL $min^{-1}$). Using 0.01 mol $L^{-1}$ $CaCl_2$ solution to back flush three columns for 10 d, the detected concentrations of SMX and TMP were, respectively, 1.1 and 0.8 μg $L^{-1}$, on the 10th day. It showed that some TMP and SMX were desorbed into water. Thus, ACST appears to have an unwanted consequence: adsorbed pollutants are likely to be desorbed into water. However, an advantage is that ACST has the capacity of regeneration.

### 3.2. Concentrations of $K^+$, $Na^+$, $Ca^{2+}$, and $Mg^{2+}$ over time

This study focused on monitoring the variation of cations ($K^+$, $Na^+$, $Ca^{2+}$, and $Mg^{2+}$) and results are described in Fig. 5.

#### 3.2.1. $Ca^{2+}$ concentration result

The $Ca^{2+}$ concentration result is described in Fig. 5(a). The $Ca^{2+}$ effluent concentrations are above 10 mg $L^{-1}$, which are significantly higher than the $Mg^{2+}$, $K^+$, and $Na^+$ effluent concentrations. Desorption from soil might be the main process because the use of 0.01 mol $L^{-1}$ $CaCl_2$ to back flush the three columns prior to the experiment result in the sorption of a large number of $Ca^{2+}$ onto soil. By monitoring $Ca^{2+}$ concentrations, effluent $Ca^{2+}$ concentrations of three columns were ranked as column 1 > column 3 > column 2, which were not corresponding to the order of infiltration rates in three columns. The high influent $Na^+$ concentrations in column 3 might directly interfere with the release of $Ca^{2+}$. The CEC of soil was higher for $H^+$ than for $Ca^{2+}$. From the pH monitoring result depicted in Fig. 3(a), the effluent pH values in the three columns were higher than the pH values of the influent. Effluent pH values occurred in the following order: column 3 > column 1 > column 2. This did not correspond with effluent $Ca^{2+}$ concentrations. Except for $H^+$ and $Na^+$, whether the removal of SMX and TMP also affected $Ca^{2+}$ effluent concentrations or not. To explain the mechanism, 0.01 mol $L^{-1}$ $CaCl_2$ solution was used to back flush for 10 d after 60-d column experiments. The detected concentrations of SMX and TMP were, respectively, 1.1 and 0.8 μg $L^{-1}$ on the 10th day. The values are little enough, compared with the value of 20 μg $L^{-1}$. Thus, back flush was stopped. Then the deionized water was used as the influent for 7 d at the flow rate of 5 mL $min^{-1}$. In this way, the variable of the material used in the columns could be excluded from factors. The results suggested that effluent $Ca^{2+}$ concentrations of the three columns occurred in the following order: column 3 > column 1 > column 2, which is different from the results of the 60-d experiments. The removal of SMX and TMP might also have affected the release of $Ca^{2+}$ into water, and some portion of the $Ca^{2+}$ might be involved in the sorption of TMP and SMX. In addition, the removed SMX and TMP concentrations and the $Ca^{2+}$ desorption concentrations were chosen to conduct the trend graph, listed in Figs. S1 and S2. On the whole, the SMX and TMP removal amount has a decline trend and the $Ca^{2+}$ desorption amount has also a decline trend with the experiment time. Thus, it is estimated that there is a correlation between the removed SMX and TMP concentrations and $Ca^{2+}$ desorption concentrations. Further, the removal of SMX and TMP might be related to $Ca^{2+}$ hydrogeological process.

#### 3.2.2. $Mg^{2+}$ concentration result

From the $Mg^{2+}$ concentration result, described in Fig. 5(b), the effluent $Mg^{2+}$ concentrations occurred in the

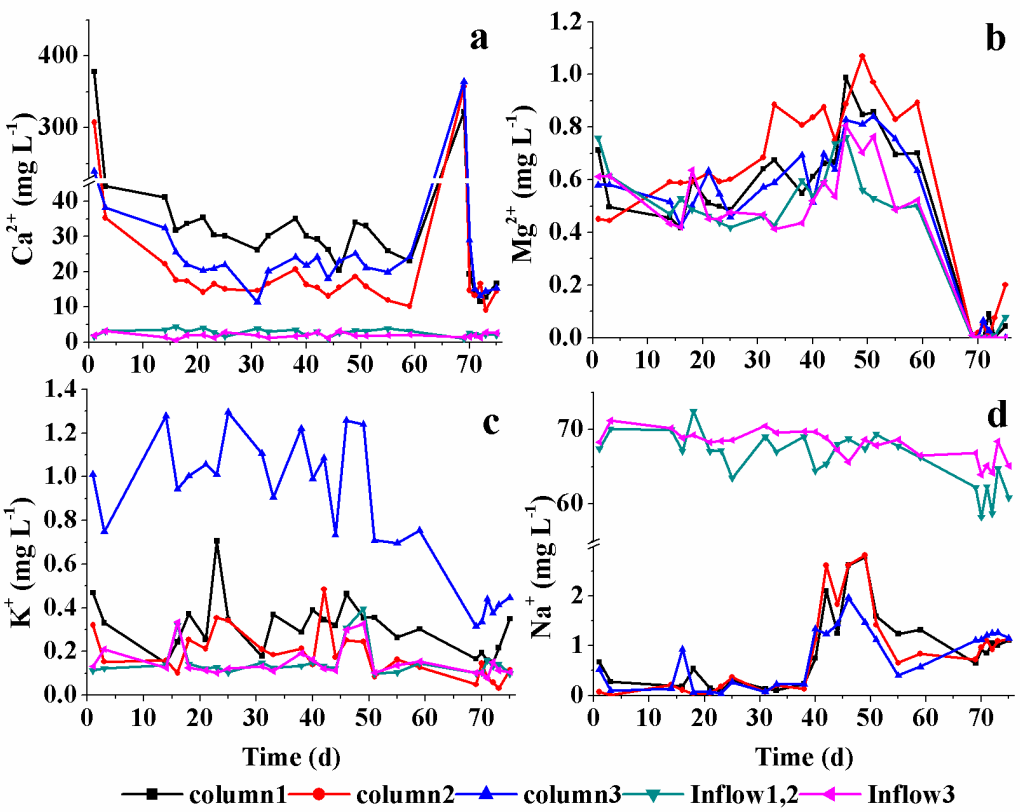


Fig. 5. The results of $Ca^{2+}$, $Mg^{2+}$, $K^+$, and $Na^+$ concentrations over time; inflow 1,2 represents the $Ca^{2+}$, $Mg^{2+}$, $K^+$, and $Na^+$ influent concentrations of columns 1 and 2. Inflow 3 represents the $Ca^{2+}$, $Mg^{2+}$, $K^+$, and $Na^+$ influent concentrations of column 3. Columns 1–3 represent the $Ca^{2+}$, $Mg^{2+}$, $K^+$, and $Na^+$ effluent concentrations of columns 1–3, respectively.

following order: column 2 > column 1 > column 3 and the effluent $Mg^{2+}$ concentrations were higher than the influent'. The phenomenon of more effluent $Mg^{2+}$ concentrations than influent' agreed with sodium/magnesium ions exchange theory, described in Eq. (1). It showed that the infiltration rate was not the main factor. The elemental analysis results of the material filled in columns were listed in Table 2; results demonstrate that the MgO contents of clay ceramsites, silty clay, and medium-coarse sands were, respectively, 0.76%, 1.43%, and 0.36%. The element Mg contents in column 2, filled with medium-coarse sands and clay ceramsites, were lower than that of columns 1 and 3. Accordingly, the effluent $Mg^{2+}$ concentrations of column 2 were lower than that of columns 1 and 3. However, the effluent $Mg^{2+}$ concentrations did not correspond with the element Mg contents. Moreover, the theory that more time for rock–water interactions result in higher dissolved ion concentrations was not supported by the observed effluent $Mg^{2+}$ concentrations. It is possible that a portion of leachable $Mg^{2+}$ participate in other actions. The most probable reason is that the formation of strong complexes with $Mg^{2+}$ occurred, or $Mg^{2+}$ played an important role in metal-bridging with anionic SMX and TMP. Because the influent water was changed, the 70–75d experimental data did not prove the conclusion.

$$2Na^{+} + Mg\ (\text{exchanged}) \rightleftharpoons Mg^{2+} + 2Na\ (\text{exchanged}) \quad (1)$$

*3.2.3. $K^{+}$ concentrations*

The $K^{+}$ concentration result is described in Fig. 5(c). Though the infiltration rates of columns 1 and 3 were comparable, effluent $K^{+}$ concentrations varied, and occurred in the following order: column 3 > column 1 > column 2; these corresponded to the SMX and TMP removal rates and infiltration rates of the three columns. We speculate, based on these results, that ion exchange action resulting from hydrogeological processes is related to the SMX and TMP removal mechanism. The SMX and TMP effluent concentrations and the $K^{+}$ effluent concentrations in columns 1–3 are chosen to conduct the trend graph, listed in Figs. S3 and S4. On the whole, the TMP effluent concentrations have a decline trend and $K^{+}$ effluent concentrations have also a decline trend over time. There is a correlation between the TMP effluent concentrations and $K^{+}$ desorption concentrations. By elemental analyzing, the material filled in columns described in Table 2, $K_2O$ contents of clay ceramsites, silty clay, and medium-coarse sands were, respectively, 2.25%, 2.86%, and 4.66%. A desorption process for soil ions can be described as Fig. 6.

To test the above two arguments, 0.01 mol $L^{-1}$ $CaCl_2$ solution was used to back flush. The effluent $K^{+}$ concentrations of the three columns were clearly lower than the effluent $K^{+}$ concentrations of the 60-d experiments. These findings suggest that a small portion of $K^{+}$ released from dissolution are derived from soil desorption, while the other portion might be affected by the removal process of TMP and SMX.

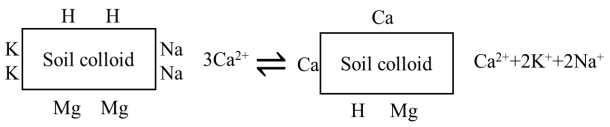


Fig. 6. A desorption process for soil ions.

*3.2.4. $Na^{+}$ concentration result*

The $Na^{+}$ concentration result is described in Fig. 5(d). Influent and effluent $Na^{+}$ concentrations were similar between columns 1 and 2. This phenomenon might be related to the CEC of soil. Because the monovalent ions had a smaller sorption energy and were therefore more likely to remain in solutions [5]. The soil CEC occurred in the following order: $H^{+} > Ca^{2+} > Mg^{2+} > K^{+} > Na^{+}$. In the presence of disseminated clay material within the aquifer, ion exchange causes $Ca^{2+}$ to be replaced by $Na^{+}$ in solutions [16]. The effluent $Na^{+}$ concentrations in column 3 were lower than the influent $Na^{+}$ concentrations. The clay mineral selectivity for cations induces a release of Ca and a trapping of Na, in contact with Na-rich water [17]. Because the influent of column 3 was supplemented with 200 mg $L^{-1}$ $NaN_3$, $Na^{+}$ was the dominant ion and the cation exchange reaction depicted in Eq. (2) can occur:

$$2Na^{+} + Ca\ (\text{exchanged}) \rightleftharpoons Ca^{2+} + 2Na\ (\text{exchanged}) \quad (2)$$

As the exchanger took up $Na^{+}$, $Ca^{2+}$ was released and the effluent $Ca^{2+}$ concentrations were increased. The effluent $Ca^{2+}$ concentrations in column 3 were lower than that of column 1, which did not agree with the $Na^{+}$ exchange results. When the influent was replaced by deionized water, effluent $Na^{+}$ concentrations in columns 1 and 3 decreased to below the influent $Na^{+}$ concentrations, while effluent $Ca^{2+}$ concentrations in columns 1 and 3 were not significantly different from one another. In contrast, the addition of $NaN_3$ inhibited the $Ca^{2+}$ desorption. The effluent $Na^{+}$ concentrations were lower than the influent $Na^{+}$ concentrations in column 3, which suggests that the added $NaN_3$ might be adsorbed on the material surface sites desorbed by $Ca^{2+}$.

*3.3. Trace elements $Fe^{3+}$, $Mn^{2+}$, $Cu^{2+}$, and $Zn^{2+}$*

$Fe^{3+}$, $Mn^{2+}$, $Cu^{2+}$, and $Zn^{2+}$ were analyzed at 16, 28, 46, and 58 d, respectively. The results are shown in Fig. 7. Elemental concentrations of Fe, Cu, Mn, and Zn were not high, and ranged from 0.04 to 2.50 μg $L^{-1}$. The effluent $Cu^{2+}$ concentrations in column 3 were higher than those of columns 1 and 2. The elemental analysis results of the material filled in columns were listed in Table 2; clay ceramsites contained 0.01% CuO, while the other materials did not contain any Cu. It indicates that the effluent $Cu^{2+}$ concentrations are significantly affected by the influent. The average effluent $Fe^{3+}$ concentrations in the three columns were higher than those of the other elements, which could be explained by the high $Fe_2O_3$ contents of clay ceramsites (16.79%), silty clay (5.5%), and medium-coarse sands (2.19%); these values are all higher than those of the other trace elements. In column 3, the high effluent $Fe^{3+}$ contents relative to other columns might be related to the lower infiltration rate, because longer hydraulic retention time allows for further ion leaching. The effluent $Mn^{2+}$ concentrations of column 3 were slightly higher than those of columns 1 and 2. The difference was not related to the material filled in

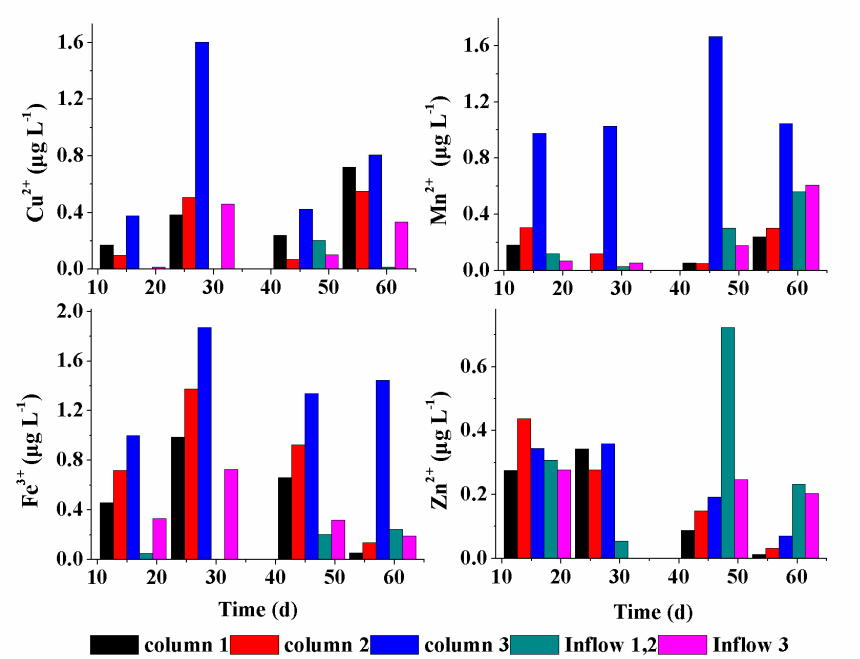


Fig. 7. The results of $Cu^{2+}$, $Fe^{3+}$, $Mn^{2+}$, and $Zn^{2+}$ concentrations over time; inflow 1,2 represents the influent $Cu^{2+}$, $Fe^{3+}$, $Mn^{2+}$, and $Zn^{2+}$ concentrations of columns 1 and 2. Inflow 3 represents the influent $Cu^{2+}$, $Fe^{3+}$, $Mn^{2+}$, and $Zn^{2+}$ concentrations of column 3. Columns 1–3 represent the effluent $Cu^{2+}$, $Fe^{3+}$, $Mn^{2+}$, and $Zn^{2+}$ concentrations of columns 1–3, respectively.

columns, because $Mn^{2+}$ contents of clay ceramsites, silty clay, and medium-coarse sands were, respectively, 0.13%, 0.09%, and 0.05%. The effluent concentrations in column 3 might be related to the infiltration rate. The $Zn^{2+}$ contents of clay ceramsites, silty clay, medium-coarse sands were 0.03%, 0.01%, and 0, respectively. Thus, $Zn^{2+}$ concentrations in all three columns were also very low, and the effluent $Zn^{2+}$ concentrations were higher than the influent $Zn^{2+}$ concentrations from 0 to 30 d, while the effluent $Zn^{2+}$ concentrations were lower than the $Zn^{2+}$ influent concentrations from 30 to 60 d. Because the influent contained some trace concentrations, the final results may be disturbed. According to "Standards for Drinking Water Quality" (GB 5749-2006) of China, $Fe^{3+}$, $Mn^{2+}$, $Cu^{2+}$, and $Zn^{2+}$ safe levels are 0.3, 0.1, 1, and 1 mg $L^{-1}$, respectively. The observed concentrations of $Fe^{3+}$, $Mn^{2+}$, $Cu^{2+}$, and $Zn^{2+}$ are low (μg $L^{-1}$ level), so they are not harmful to human health.

## 4. Conclusion

This work systematically investigated the removal of SMX and TMP by ACST with different high infiltration rates with a broad range of hydrogeological indexes including: $K^+$, $Na^+$, $Ca^{2+}$, $Mg^{2+}$, $Fe^{3+}$, $Mn^{2+}$, $Cu^{2+}$, and $Zn^{2+}$. Results of this study revealed that ACST with high infiltration rates improved the removal rates of SMX and TMP, which both increased by about 20%, and the removal rate of TMP was higher than that of SMX. Effluent $Ca^{2+}$ concentrations occurred in the following order: column 1 > column 3 > column 2. This suggests that the high influent $Na^+$ concentrations might directly hinder the release of $Ca^{2+}$, and $Ca^{2+}$ might participate in the SMX and TMP removal by back flushing and changing influent to deionized water. Results on $K^+$ concentrations demonstrate that a small portion of the $K^+$ released by dissolution might be derived from soil desorption, while the remaining portion may be related to the removal of TMP and SMX. However, results on the effluent $Mg^{2+}$ concentrations supported the sodium/magnesium ions exchange theory. In principle, removal processes of SMX and TMP have the relationship with hydrogeochemical processes of $K^+$, $Na^+$, $Ca^{2+}$, and $Mg^{2+}$. The effluent $Fe^{3+}$, $Mn^{2+}$, $Cu^{2+}$, and $Zn^{2+}$ concentrations were low (μg $L^{-1}$ level), which did not cause secondary water pollution.

## Acknowledgments

The authors thank Beijing Natural Science Foundation (J150004), Key technology and project of Jinan water environment control (No. 201509002), the National Natural Science Foundation of China (No. 51378287), and Key Project of Natural Science Foundation of China (41130637) for the financial support of this work.

## References

[1] K. Pholkern, K. Srisuk, T. Grischek, M. Soares, S. Schäfer, L. Archwichai, P. Saraphirom, P. Pavelic, W. Wirojanagud, Riverbed clogging experiments at potential river bank filtration sites along the Ping River, Chiang Mai, Thailand, Environ. Earth Sci., 73 (2015) 7699–7709.

[2] Q. Liu, M. Li, F. Zhang, H. Yu, Q. Zhang, X. Liu, The removal of trimethoprim and sulfamethoxazole by a high infiltration rate artificial composite soil treatment system, Front. Environ. Sci. Eng., 11 (2017) 12.

[3] X. Wang, H. Yang, Z. Li, S. Yang, Y. Xie, Pilot study for the treatment of sodium and fluoride-contaminated groundwater by using high-pressure membrane systems, Front. Environ. Sci. Eng., 9 (2015) 155–163.

[4] T. Heberer, G. Massmann, B. Fanck, T. Taute, U. Dünnbier, Behaviour and redox sensitivity of antimicrobial residues during bank filtration, Chemosphere, 73 (2008) 451–460.

[5] W. Back, R.A. Freeze, Chemical Hydrogeology, Hutchinson Ross Publishing Company, USA, 1983.
[6] V.B. Singh, A.L. Ramanathan, J.G. Pottakkal, P. Sharma, A. Linda, M.F. Azam, C. Chatterjee, Chemical characterisation of meltwater draining from Gangotri Glacier, Garhwal Himalaya, India, J. Earth Syst. Sci., 121 (2012) 625–636.
[7] V.B. Singh, A. Ramanathan, T. Kuriakose, Hydrogeochemical assessment of meltwater quality using major ion chemistry: a case study of Bara Shigri Glacier, Western Himalaya, India, Natl. Acad. Sci. Lett., 38 (2015) 147–151.
[8] M.B. Ahmed, J.L. Zhou, H.H. Ngo, W. Guo, Adsorptive removal of antibiotics from water and wastewater: progress and challenges, Sci. Total Environ., 523 (2015) 112–126.
[9] A.M. Roussel, R.A. Anderson, A.E. Favrier, Determination of Heavy Metals in Calcium and Herbal Supplements Utilizing Inductively Coupled Plasma Mass Spectrometry (ICP-MS), Trace Elements in Man and Animals 10, Springer US, Boston, MA, 2000.
[10] P.R. Haddad, Ion chromatography, Anal. Bioanal. Chem., 379 (2004) 341–343.
[11] B. Baumgarten, J. Jährig, T. Reemtsma, M. Jekel, Long term laboratory column experiments to simulate bank filtration: factors controlling removal of sulfamethoxazole, Water Res., 45 (2011) 211–220.
[12] S.K. Maeng, S.K. Sharma, K. Lekkerkerker-Teunissen, G.L. Amy, Occurrence and fate of bulk organic matter and pharmaceutically active compounds in managed aquifer recharge: a review, Water Res., 45 (2011) 3015–3033.
[13] V.A. Tzanakakis, N.V. Paranychianakis, A.N. Angelakis, Nutrient removal and biomass production in land treatment systems receiving domestic effluent, Ecol. Eng., 35 (2009) 1485–1492.
[14] A. Dan, Y. Yang, Y. Dai, C. Chen, S. Wang, R. Tao, Removal and factors influencing removal of sulfonamides and trimethoprim from domestic sewage in constructed wetlands, Bioresour. Technol., 146 (2013) 363–370.
[15] K.S. Jewell, S. Castronovo, A. Wick, P. Falås, A. Joss, T.A. Ternes, New insights into the transformation of trimethoprim during biological wastewater treatment, Water Res., 88 (2016) 550–557.
[16] S. Chidambaram, P. Anandhan, M.V. Prasanna, K. Srinivasamoorthy, M. Vasanthavigar, Major ion chemistry and identification of hydrogeochemical processes controlling groundwater in and around Neyveli Lignite Mines, Tamil Nadu, South India, Arab. J. Geosci., 6 (2013) 3451–3467.
[17] A.P. Barker, R.J. Newton, S.H. Bottrell, J.H. Tellam, Processes affecting groundwater chemistry in a zone of saline intrusion into an urban sandstone aquifer, Appl. Geochem., 13 (1998) 735–749.

# Supplementary

## 1. Experimental section

### 1.1. Chemicals and reagents

SMX, TMP were from Dr. Ehrenstorfer (Augsburg, Germany), with purity >99%. HPLC/MS/MS methanol and acetonitrile were from Merck (Darmstadt, Germany). Formic acid, sodium azide ($NaN_3$) was purchased from Fisher Scientific (Pittsburgh, PA, USA). Milli-Q water (18.2 MΩ) was produced from a Millipore purification system (Millipore, USA). Individual stock solutions of sulfonamide antibiotics were prepared by dissolving 0.05 mg of two compounds in 50 mL of methanol in amber bottles and stored in dark at –20°C. Working solutions were prepared by dilution of stock solutions of with Milli-Q water prior to each experimental run. Deionized water was produced by Aquapro (AR2-100L-P00, containing some ions with low concentration as a result of long-time using). Ion chromatography instrument is made by Dionex (Sunnyvale, USA). The model number of positive ion chromatography is, respectively, dionex ICS1000. Inductively coupled plasma mass spectrometry is from Thermo fisher Scientific, Germany, and the model number is X Series 2. 1 g $L^{-1}$ standard solutions of $K^+$, $Na^+$, $Ca^{2+}$, $Mg^{2+}$, $Fe^{3+}$, $Mn^{2+}$, $Cu^{2+}$, and $Zn^{2+}$ are from National Center of Analysis and Testing for Nonferrous Metals and Electronic Materials.

### 1.2. Preparation of artificial composite soil column studies

The outlet of each artificial composite soil column (ASC) was connected to a capped 200 mL amber bottle. 20 L of deionized water with SMX and TMP was mixed and quickly stirred to be used as the influent by a pump at a constant flow rate (5 mL $min^{-1}$). After the ASCs were set up, 0.01 mol $L^{-1}$ $CaCl_2$ deionized solution was used to back flush ASCs for 14 d, then conducted the removal experiments for 60 d. Following the 60 d experiments, deionized water was used as the influent for 7 d. All ASCs were filled with clay ceramsites, silty clay, and medium-coarse sands. Medium-coarse sands and silty clay were cleaned, homogenized, and sieved through 1 mm and 0.2 mm meshes, respectively.

The ASCs contained four components (from the bottom up): the supporting layer (15 cm), the lower layer (25 cm), the upper layer (15 cm), and the overflow layer (10 cm). 2–5 cm of graded cobblestones were used to fill the supporting layer and a filter screen was placed above the supporting layer to prevent clay ceramsites from leaking downward. The lower layer contained clay ceramsites, and a filter screen was also placed above this layer. In the upper layer, different proportions of silty clay and medium-coarse sands were mixed.

After cleaning the ASCs with a 0.01 mol $L^{-1}$ $CaCl_2$ solution for 14 d, the infiltration rates and average porosities of the three columns were measured, as indicated in Table 4. The ASCs were operated for 1 day, then they were not operated the following day. This pattern was continued so that the ASCs were operated for 60 days between February 1 and April 1, 2016. The ASC influent and effluent were sampled after columns had been in operation for 1 h. When the volume of the water samples reached 100 mL following filtration through Whatman glass fiber filters (0.22 μm), water sample was taken out and stored at 4°C.This process was considered as a complete sampling process. The laboratory temperature is about 20°C. The removal percentage ($R$%) of antibiotics was calculated using Eq. (S1), where $C_0$ is the inflow antibiotic concentration (μg $L^{-1}$), $C_e$ is the effluent antibiotic concentration in solution (μg $L^{-1}$).

$$R\% = [(C_0 - C_e) / C_0] \times 100 \quad \text{(S1)}$$

### 1.3. The sorption experiments

#### 1.3.1. The kinetics of sorption

The kinetics of sorption determines the rate of antibiotic removal from water. In the sorption dynamics experiments, with the solid: solution ratio (1:50 for SMX and 1:100 for TMP), weigh 5 and 2.5 g clay ceramsites and put clay ceramsites in 500 mL ground-glass conical flask packed up with tinfoil to prevent the photodegradation. The initial solution concentration is 1 mg $L^{-1}$. All the samples were incubated at 25 ± 1°C, being orbitally shaken at 150 rpm for 100 h in the dark. Grab samples with 1mL injection syringes and filter samples through the Whatman glass fiber filters (0.22 μm) at 2 min, 5 min, 10 min, 15 min, 30 min, 1 h, 2 h, 4 h, 8 h, 12 h, 24 h, 28 h, 32 h, 36 h, 48 h, 60 h, 72 h, 84 h, and 100 h.

#### 1.3.2. The isotherm sorption experiments

In the isotherm sorption experiments, 50-mL amber environmental plastic addictives (EPA) vials equipped with a polytetrafluoroethylene-lined screw caps were filled with 0.25 g (0.5 g) clay ceramsites and spiked with 25 mL TMP (SMX) concentration levels: 10, 20, 50, 80, 100, 200, 400, 600, and 800 ppb. Blank control samples were also done. All the samples were also incubated at 25 ± 1°C while being orbitally shaken at 150 rpm for 100 h in the dark. After incubation, all samples were centrifuged at 3,000 rpm for 15 min, extracted with 1 mL injection syringes, and filtered through the Whatman glass fiber filters (0.22 μm).

## 2. Results and discussion

The SMX and TMP removal concentrations and the $Ca^{2+}$ desorption concentrations in columns 1–3 to conduct the trend graph, listed in Figs. S1 and S2. The SMX and TMP effluent concentrations and the $K^+$ effluent concentrations in columns 1–3 are chosen to conduct the trend graph, listed in Figs. S3 and S4.

Table S1
Gradient elution program

| Time (min) | Mobile phase (A) | Mobile phase (B) |
|---|---|---|
| 0 | 10% | 90% |
| 4 | 90% | 10% |
| 5 | 90% | 10% |
| 5.5 | 10% | 90% |
| 7 | 10% | 90% |

"A" represents Milli-Q water added 0.1% formic acid. "B" represents acetonitrile.

Table S2
Antibiotics working parameters in mass spectrum

| Sulfonamides | Precursor ion (m/z) | Product ion (m/z) | Cone voltage (v) | Collision energy (eV) | Dwell time (s) |
|---|---|---|---|---|---|
| SMX | 254.10 | 156.00 | 46.00 | 28.00 | 0.20 |
| TMP | 291.40 | 123.00 | 40.00 | 22.00 | 0.24 |

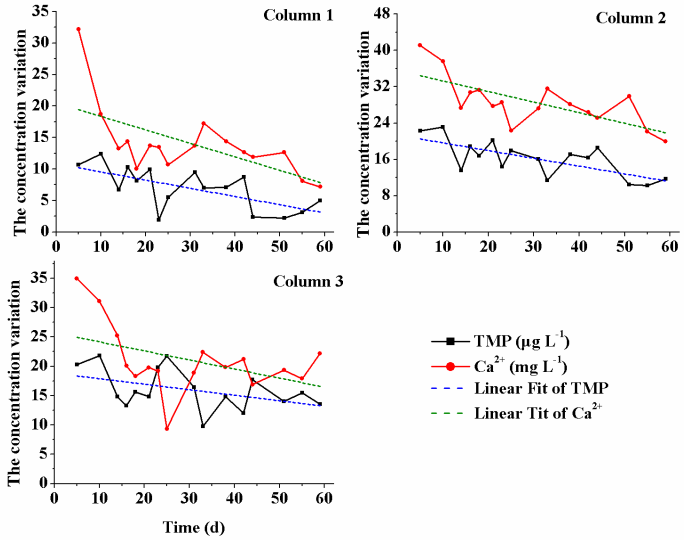


Fig. S1. The trend graph describes the trend of removed TMP concentrations and the desorption $Ca^{2+}$concentrations from the ASCT.

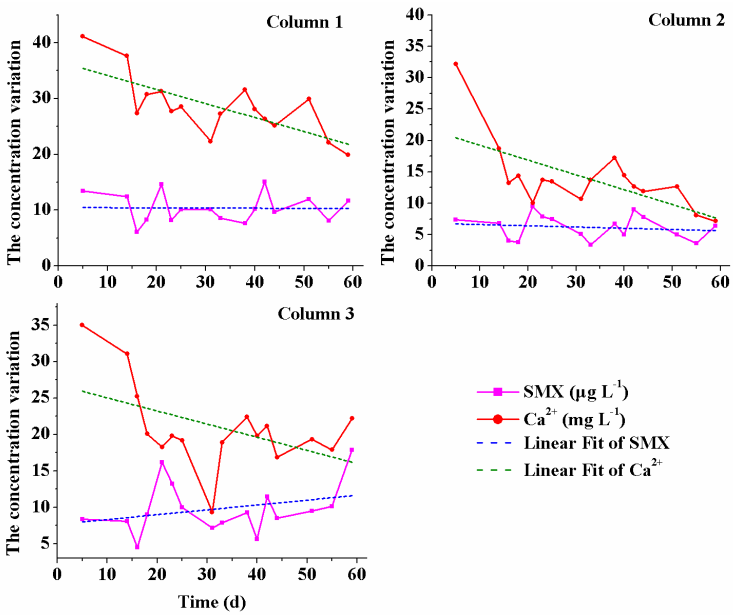


Fig. S2. The trend graph describes the trend of removed SMX concentrations and the desorption $Ca^{2+}$ concentrations from the ASCT.

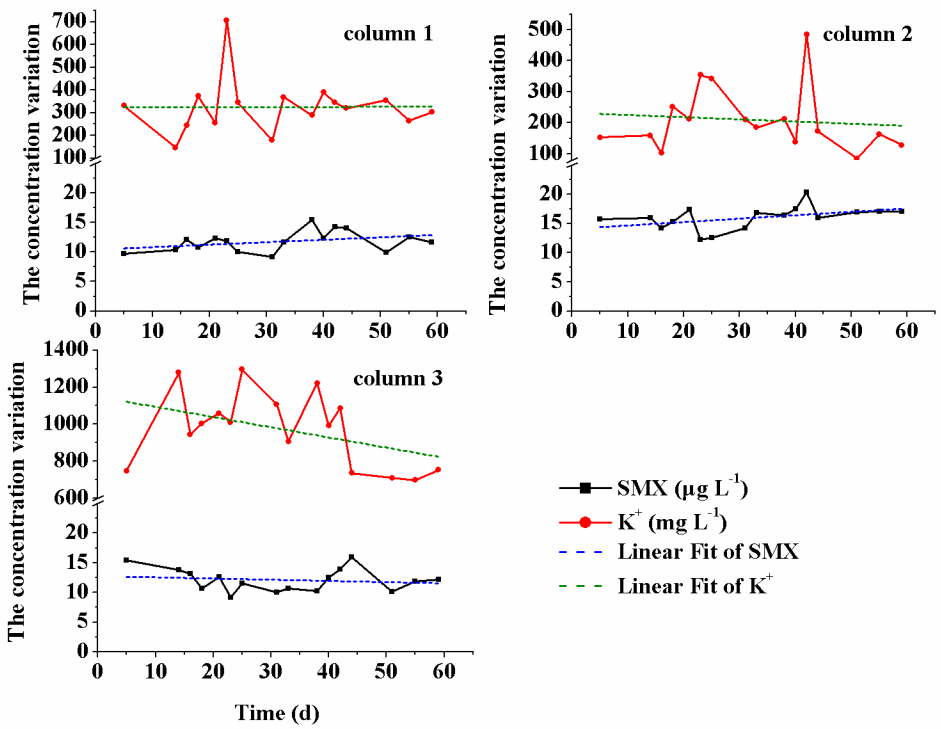


Fig. S3. The trend graph describes the trend of SMX effluent concentrations and the effluent $K^+$ concentrations.

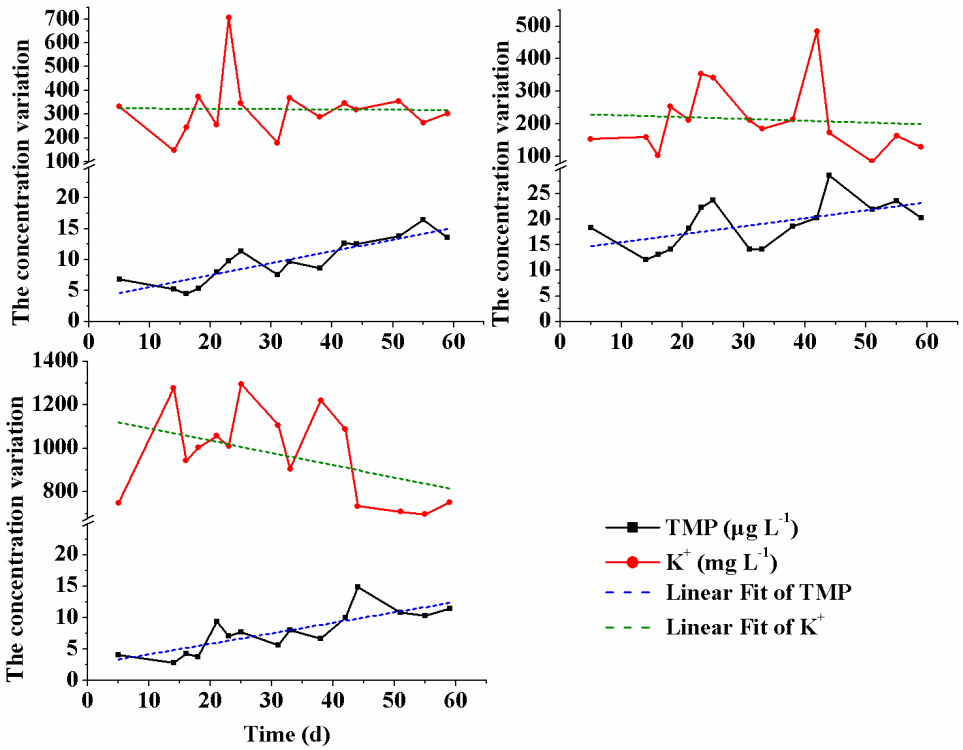


Fig. S4. The trend graph describes the trend of effluent TMP concentrations and the effluent $K^+$ concentrations.